

# Acoustic phonon-limited resistivity in spin-orbit coupled 2DEG: Deformation potential and piezoelectric scattering

Tutul Biswas and Tarun Kanti Ghosh

*Department of Physics, Indian Institute of Technology-Kanpur, Kanpur-208 016, India*

(Dated: June 24, 2018)

We study the interaction between electron and acoustic phonon in a Rashba spin-orbit coupled two dimensional electron gas using Boltzmann transport theory. Both deformation potential and piezoelectric scattering mechanisms are considered in the Bloch-Gruneisen (BG) as well as in the equipartition (EP) regimes. Effect of the Rashba spin-orbit interaction on the temperature dependence of resistivity in the BG and EP regimes has been discussed. We find effective exponent of the temperature dependence of the resistivity in the BG regime decreases due to spin-orbit coupling.

PACS numbers: 71.38.-k, 71.70.Ej, 72.20.Dp

## I. INTRODUCTION

With the rise of the promising field of spintronics, two dimensional electron gas (2DEG) with spin-orbit interaction (SOI) in semiconductor heterostructures has drawn much attention in recent years<sup>1-3</sup>. The importance of this field was first realized when Datta and Das gave a proposal of Spin Field Effect Transistor<sup>4</sup>. Several studies on spintronics have been performed in recent years from both theoretical and experimental viewpoints. One major aim is to manipulate the spin degree of freedom of charge carriers in semiconductor nanostructures<sup>5</sup> so that spin-based device technology<sup>6</sup> and quantum information processing<sup>7</sup> can be developed in near future. The SOI is an intrinsic phenomena present in semiconductors. Mainly, there are two kinds of SOI present in the semiconductor heterostructures we come across in the literature. One of them is the Rashba spin-orbit interaction (RSOI)<sup>8</sup> which originates from the inversion asymmetry of the confining potential in semiconductor heterostructures. The RSOI is proportional to the magnitude of the electric field internally generated due to the band bending or externally applied gate voltage. It can be tuned by applying a gate voltage<sup>9,10</sup>. Another kind of SOI is the Dresselhaus spin-orbit interaction<sup>11</sup> which originates from the bulk inversion asymmetry of the host crystal. It entirely depends on crystal property and it is not tunable.

Various electronic and transport properties of a 2DEG will be modified in the presence of the SOI. We mainly focus on the RSOI in 2DEG systems such as AlGaAs/GaAs heterostructure. The coupling between electron and phonon becomes stronger when the SO coupling constant is large enough and due to this fact the effective mass is also increased<sup>12</sup>. The critical temperature of superconductors can be controlled by RSOI when the Fermi energy is small as compared to the characteristic energy scale of RSOI<sup>13</sup>. The RSOI can produce infinite number of bound states in a 2DEG with short-range impurity potentials<sup>14</sup>. At low frequency in the presence of RSOI the universality of spin Hall conductivity can be broken by considering the contribution of electron-phonon interaction to the spin-vertex correction<sup>15</sup>. The mobility, polaron mass

correction and polaron binding energy can be changed significantly due to the presence of the RSOI<sup>16,17</sup>. The relaxation time for various impurity potentials of low-dimensional semiconductor structures with SOI has been studied<sup>18</sup>.

The interaction between electron and phonon plays a very crucial role in determining the transport properties of a 2DEG and it has a finite contribution to the momentum relaxation time of the charge carriers. Other contributions<sup>19-23</sup> come from disorders, impurities, etc. There are three distinct temperature regimes: a) Bloch-Gruneisen (BG), b) Equipartition (EP) and c) Inelastic phonon scattering. The BG temperature  $T_{BG}$  can be defined<sup>24</sup> by the relation  $k_B T_{BG} = 2\hbar k_F v_s$ , where  $k_B$  is the Boltzmann constant,  $v_s$  is the phonon velocity and  $k_F$  is the Fermi wave vector. For typical electron density ( $n_e \sim 10^{15} \text{ m}^{-2}$ ) in a 2DEG system,  $T_{BG}$  is around 6.2 K. In the BG regime, a direct manifestation of the acoustic phonon-dominated transport property is the strong change in the temperature dependence of the resistivity. The existence of the BG regime has been confirmed for 2DEG experimentally<sup>24</sup>. The problem of electron-phonon interaction in a 2DEG confined in semiconductor heterostructures has been studied extensively<sup>25-32</sup>. Recently, the phonon-dominated transport properties in the BG regime have been studied in graphene both theoretically<sup>33-35</sup> and experimentally<sup>36</sup>.

In the present work we would like to investigate the influence of the RSOI on momentum relaxation time due to electron-phonon interaction and hence on the transport properties of 2DEG systems. We consider both the cases for perfect 2DEG and quasi-2DEG (usually found in semiconductor heterostructures). In the former case 2D phonon wave vector  $\mathbf{q}$  couples with 2D electron wave vector  $\mathbf{k}$  and in the latter case the coupling between 3D bulk phonon wave vector  $\mathbf{Q} = (\mathbf{q}, q_z)$  and 2D electron wave vector  $\mathbf{k}$  is considered. We consider two mechanisms of electron-phonon interaction, namely deformation potential (DP) and piezoelectric (PE) potential scattering separately. In all the cases linear temperature dependence of inverse relaxation time (IRT) is found in the high temperature (EP) regime. But in the BG regime for perfect 2DEG and quasi-2DEG we find analytically

resistivity is proportional to  $T^4$  and  $T^5$ , respectively, in the case of DP scattering mechanism. On the other hand,  $\rho \sim T^3$  for PE scattering mechanism in a quasi-2DEG. Our numerical calculations reveal that this exponent of  $T$  *strongly* depends on density and the SO coupling constant. In fact, the exponent of  $T$  decreases due to presence of spin-orbit coupling. We also discuss the resistivity as a function of the SO coupling constant in the BG and EP regimes.

This paper is organized as follows. In section II we derive all the theoretical results and discuss all the numerical analysis for perfect 2DEG. In section III both DP and PE scattering mechanisms have been taken into account for quasi-2DEG and we discuss analytical and numerical results in detail. We summarize all the results in section IV.

## II. ELECTRON-PHONON SCATTERING IN A PERFECT 2DEG

### A. Theoretical model

We consider a 2DEG with the RSOI in the  $xy$  plane in a semiconductor heterostructure. The single-particle Hamiltonian of this system is given by

$$H = \frac{\mathbf{p}^2}{2m^*} \sigma_0 + \frac{\alpha}{\hbar} (\sigma_x p_y - \sigma_y p_x), \quad (1)$$

where  $\mathbf{p}$  is the two-dimensional momentum operator,  $m^*$  is the effective mass of an electron,  $\sigma_0$  is the unit  $2 \times 2$  matrix,  $\alpha$  is the Rashba spin-orbit coupling constant and  $\sigma_{x(y)}$  are the Pauli matrices. The eigenenergies are given by

$$\epsilon_\lambda(k) = \frac{\hbar^2 k^2}{2m^*} + \lambda \alpha |\mathbf{k}|, \quad (2)$$

with the corresponding normalized eigenspinors

$$\psi_\lambda(x, y) = \frac{1}{\sqrt{2A}} \begin{pmatrix} 1 \\ \lambda e^{-i\phi} \end{pmatrix} e^{i\mathbf{k} \cdot \mathbf{r}}. \quad (3)$$

Here,  $\lambda = \pm$  represents the upper and lower energy branches,  $A$  is the area of the system and  $\phi = \tan^{-1}(k_x/k_y)$ . The density of states for the two energy branches are given by<sup>12</sup>

$$D_\pm(\epsilon) = \frac{D_0}{2} \left( 1 \mp \sqrt{\frac{\epsilon_\alpha}{\epsilon + \epsilon_\alpha}} \right) \Theta(\epsilon) + D_0 \sqrt{\frac{\epsilon_\alpha}{\epsilon + \epsilon_\alpha}} \Theta(-\epsilon) \Theta(\epsilon + \epsilon_\alpha). \quad (4)$$

Here,  $D_0 = m^*/(\pi \hbar^2)$ ,  $\Theta(x)$  is the unit step function and  $\epsilon_\alpha = m^* \alpha^2 / (2 \hbar^2)$  is the characteristic energy scale of RSOI.

The Hamiltonian for electron-phonon interaction in the case of deformation potential coupling can be written as

$H_{\text{ep}} = D \nabla \cdot \mathbf{u}(\mathbf{r})$ , where  $D$  is the deformation-potential coupling constant and the lattice displacement vector  $\mathbf{u}(\mathbf{r})$  is given by

$$\mathbf{u}(\mathbf{r}) = \sum_{\mathbf{q}} \sqrt{\frac{\hbar}{2MN\omega_{\mathbf{q}}}} \mathbf{e}_{\mathbf{q}} [a_{\mathbf{q}} e^{i\mathbf{q} \cdot \mathbf{r}} + a_{\mathbf{q}}^\dagger e^{-i\mathbf{q} \cdot \mathbf{r}}]. \quad (5)$$

Here,  $\omega_{\mathbf{q}} = v_s q$  is the phonon frequency with the wave vector  $q$  and the sound velocity  $v_s$ ,  $a_{\mathbf{q}}^\dagger$  and  $a_{\mathbf{q}}$  are phonon creation and annihilation operators, respectively. Also,  $\mathbf{e}_{\mathbf{q}}$  is a unit vector in the direction of the phonon polarization. The corresponding Hamiltonian can be written as

$$H_{\text{ep}}(\mathbf{r}) = \sum_{\mathbf{q}} [C_{\mathbf{q}} a_{\mathbf{q}} e^{i\mathbf{q} \cdot \mathbf{r}} + C_{\mathbf{q}}^\dagger a_{\mathbf{q}}^\dagger e^{-i\mathbf{q} \cdot \mathbf{r}}], \quad (6)$$

where  $C_{\mathbf{q}} = D \sqrt{\hbar/2MN\omega_{\mathbf{q}}} (i\mathbf{e}_{\mathbf{q}} \cdot \mathbf{q})$ .

The energy dependent relaxation time for electrons in a given energy branch  $\lambda$  can be written as

$$\frac{1}{\tau^\lambda(\epsilon)} = \sum_{\mathbf{k}', \lambda'} (1 - \cos \theta_{\mathbf{k}\mathbf{k}'}) P_{\mathbf{k}\mathbf{k}'}^{\lambda\lambda'} \frac{1 - f(\epsilon_{\lambda'}(k'))}{1 - f(\epsilon_\lambda(k))}, \quad (7)$$

where  $\theta_{\mathbf{k}\mathbf{k}'}$  is the scattering angle between the two momentum vectors  $\mathbf{k}$  and  $\mathbf{k}'$ ,  $\epsilon_\lambda$  is given by Eq. (2),  $P_{\mathbf{k}\mathbf{k}'}^{\lambda\lambda'}$  is the transition rate for scattering of an electron from a state  $|\mathbf{k}, \lambda\rangle$  to  $|\mathbf{k}', \lambda'\rangle$  and  $f(\epsilon) = [e^{\beta(\epsilon - \mu)} + 1]^{-1}$  is the Fermi-Dirac distribution function with  $\beta = 1/(k_B T)$ . The chemical potential  $\mu$  at finite temperature  $T$  can be obtained self-consistently from the following normalization condition<sup>37</sup>:

$$n_e = \int_0^\infty d\epsilon D_0 f(\epsilon) + \int_{-\epsilon_\alpha}^0 d\epsilon D_0 f(\epsilon) \sqrt{\frac{\epsilon_\alpha}{\epsilon + \epsilon_\alpha}}, \quad (8)$$

where  $n_e$  is the electron density. At  $T = 0$ , the above equation reduces to  $\epsilon_F = \epsilon_F^0 - 2\epsilon_\alpha$ , where  $\epsilon_F$  and  $\epsilon_F^0$  is the Fermi energy of a 2DEG in presence and absence of RSOI, respectively. Thus, the reduction in the Fermi energy due to RSOI is  $2\epsilon_\alpha$ .

We consider the interaction between electron and acoustic phonon due to deformation potential coupling. The transition rate due to electron-phonon interaction can be written as

$$P_{\mathbf{k}\mathbf{k}'}^{\lambda\lambda'} = \frac{2\pi}{\hbar} \sum_{\mathbf{q}} |C_{\mathbf{q}}^{\lambda\lambda'}|^2 \left[ N_{\mathbf{q}} \delta(\epsilon'_{\lambda'} - \epsilon_\lambda - \hbar\omega_{\mathbf{q}}) + (N_{\mathbf{q}} + 1) \delta(\epsilon'_{\lambda'} - \epsilon_\lambda + \hbar\omega_{\mathbf{q}}) \right], \quad (9)$$

where  $C_{\mathbf{q}}^{\lambda\lambda'}$  is the matrix element for the acoustic phonon and is given by

$$|C_{\mathbf{q}}^{\lambda\lambda'}|^2 = \frac{D^2 \hbar q}{2A \rho_a v_s} \frac{1 + \lambda \lambda' \cos \theta}{2} \delta_{\lambda\lambda'}. \quad (10)$$

Here,  $\theta \equiv \theta_{\mathbf{k}\mathbf{k}'}$ ,  $D$  is the deformation potential coupling constant and  $\rho_a = NM/A$  is the mass per unit area. The

appearance of  $\delta_{\lambda\lambda'}$  is due to the fact that the electron-phonon interaction given by Eq. (6) is spin-independent. Also,  $N_{\mathbf{q}} = [\exp(\beta\hbar\omega_{\mathbf{q}}) - 1]^{-1}$  is the phonon occupation number. The first and second terms on the right hand side of Eq. (9) correspond to the absorption and emission of a phonon with energy  $\hbar\omega_{\mathbf{q}}$ , respectively. Within the small-angle scattering approximation ( $q = 2k \sin(\theta/2)$ ), the matrix element for intra-branch scattering ( $\lambda = \lambda'$ ) becomes  $|C_{\mathbf{q}}^{\lambda\lambda'}|^2 = \frac{D^2\hbar q}{2A\rho_a v_s} (1 - \frac{q^2}{4k^2})$ . The similar matrix element is obtained for a single layer graphene<sup>33</sup>.

Before presenting the numerical results, we present how IRT depends on  $T$  in the EP and the BG regimes. At high temperature (EP regime), the phonon energy is much smaller than the thermal energy i.e.  $\hbar\omega_{\mathbf{q}} \ll k_B T$ . We neglect  $\hbar\omega_{\mathbf{q}}$  term in the delta functions i.e.  $\delta(\epsilon' - \epsilon \mp \hbar\omega_{\mathbf{q}}) \simeq \delta(\epsilon' - \epsilon)$ . Again, in this temperature limit the Bose occupation factor  $N_{\mathbf{q}}$  can be approximated as  $N_{\mathbf{q}} \simeq N_{\mathbf{q}} + 1 \simeq k_B T / \hbar\omega_{\mathbf{q}}$ . When  $\epsilon_F \geq \epsilon_{\alpha}$ , the total relaxation time at high temperature is

$$\frac{1}{\tau(\epsilon)} \simeq \frac{m^* D^2}{2\rho_a \hbar^3 v_s^2} k_B T. \quad (11)$$

Therefore, in the EP regime, the IRT depends linearly on temperature.

Now we want to see how resistivity depends on temperature and  $\alpha$  at low temperature (BG regime) where  $\hbar\omega_{\mathbf{q}} \sim k_B T$ . In the BG regime, the IRT strongly decreased because the phonon population decreases exponentially for phonon absorption and the sharp Fermi distribution prohibits phonon emission. To see the temperature dependence of the resistivity in the BG regime, it is convenient to calculate IRT averaged over energy, as used for graphene<sup>33</sup>, which is given by

$$\left\langle \frac{1}{\tau^{\lambda}} \right\rangle = \frac{\int d\epsilon D_{\lambda}(\epsilon) \frac{1}{\tau^{\lambda}} \left[ -\frac{df(\epsilon)}{d\epsilon} \right]}{\int d\epsilon D_{\lambda}(\epsilon) \left[ -\frac{df(\epsilon)}{d\epsilon} \right]}. \quad (12)$$

Therefore, the resistivity of a 2DEG with RSOI can be calculated from the following equation:

$$\rho = \frac{m^*}{n_e e^2} \left\langle \frac{1}{\tau} \right\rangle, \quad (13)$$

where  $\langle 1/\tau \rangle = \sum_{\lambda} \langle 1/\tau^{\lambda} \rangle$ .

When the temperature is very low we can make the following approximations: (i) the phonon energy is comparable to the thermal energy i.e.  $k_B T \leq \hbar\omega_{\mathbf{q}} \ll \epsilon_F$  and  $f(\epsilon)[1 - f(\epsilon \pm \hbar\omega_{\mathbf{q}})] \simeq \hbar\omega_{\mathbf{q}} (N_{\mathbf{q}} + 1/2 \pm 1/2) \delta(\epsilon - \epsilon_F)$ . After taking these approximations, we obtain

$$\begin{aligned} \left\langle \frac{1}{\tau^{\pm}} \right\rangle &\simeq \frac{2AD_0}{k_B T} \left( 1 \mp \sqrt{\frac{\epsilon_{\alpha}}{\epsilon_F + \epsilon_{\alpha}}} \right) \\ &\times \int_0^{\pi} d\theta (1 - \cos\theta) |C_{\mathbf{q}}|^2 \omega_{\mathbf{q}} N_{\mathbf{q}} (N_{\mathbf{q}} + 1). \end{aligned} \quad (14)$$

We can now convert the integration over  $\theta$  into  $q$  by using the relation (based on small-angle scattering)  $q =$

$2k_F \sin \frac{\theta}{2}$ . Substituting this and after a straightforward calculation we finally obtain

$$\left\langle \frac{1}{\tau^{\pm}} \right\rangle \simeq \frac{D_0}{2} \left( 1 \mp \sqrt{\frac{\epsilon_{\alpha}}{\epsilon_F + \epsilon_{\alpha}}} \right) \frac{D^2}{\rho_a v_s} \frac{4! \zeta(4)}{(v_s \hbar)^4} \frac{(k_B T)^4}{(k_F^{\pm})^3}, \quad (15)$$

where  $k_F^{\pm} = \sqrt{k_F^{0,2} - k_{\alpha}^2 \mp k_{\alpha}}$ ,  $k_{\alpha} = m^* \alpha / \hbar^2$  is the Rashba wave vector,  $k_F^0 = \sqrt{2\pi n_e}$  is the Fermi wave vector of a 2DEG without RSOI and  $\zeta(4) = \pi^4 / (90)$ . In this temperature regime energy averaged IRT is proportional to  $T^4$  and hence  $\rho \sim T^4$ . The  $T^4$  scaling law is also found in other perfect 2D system such as graphene<sup>33</sup>. As we will see in the numerical calculations, the exponent of the temperature dependence of the resistivity is reduced due to SOI coupling.

## B. Numerical results

In this section we determine the IRT, resistivity and their dependence on energy, temperature, SOI coupling constant etc. We solve Eq. (7) numerically. For our numerical calculation, we use  $m^* = 0.067m_0$  with  $m_0$  is the free electron mass,  $\alpha = \alpha_0 = 10^{-11}$  eV-m,  $v_s = 5.3 \times 10^3$  ms<sup>-1</sup> and the electron density  $n_0 = 10^{15}$  m<sup>-2</sup>.

In Fig. 1 we have plotted IRT as a function of energy at a fixed temperature  $T = 1$  K for densities  $n_e = n_0$  and  $n_e = 5n_0$ . It could be seen from Fig. 1 that there is a dip in the IRT. The dip occurs due to the sharpness of the Fermi distribution function at low enough temperature. It is clear from Fig. 1 that the dip occurs exactly at  $\epsilon = \epsilon_F^0$  when  $\alpha = 0$ . As  $\alpha$  increases the position of the dip appearing at energies lower than  $\epsilon_F^0$ . The dip occurs when  $\epsilon = \mu$ , where  $\mu$  is the chemical potential which we evaluate numerically by solving Eq. (8). For the electron density  $n_0$ , the Fermi energy without RSOI is  $\epsilon_F^0 = 3.6$  meV. When  $\alpha = 0$ ,  $\mu = \epsilon_F^0 = 3.6$  meV. When  $\alpha = 3\alpha_0$ ,  $\epsilon_F = 2.8$  meV and  $\mu = 0.8\epsilon_F^0$  so the dip occurs exactly at  $\epsilon = 0.8\epsilon_F^0$ . Similarly, for  $\alpha = 5\alpha_0$ ,  $\epsilon_F = 1.4$  meV and  $\mu = 0.4\epsilon_F^0$  and consequently the dip occurs exactly at  $\epsilon = 0.4\epsilon_F^0$ . The IRT of the 2DEG system with RSOI is reduced compared to the absence of SOI.

The effective exponent ( $\nu$ ) of the temperature dependence of the resistivity strongly depends on the density and the RSOI coupling constant. We estimate the effective exponent from the log-log plot of the resistivity versus  $T$  in Fig. 2 for  $\alpha = 0$  and  $\alpha = \alpha_0$  with different densities. In the BG regime ( $T \sim 1 - 3$  K), we find  $\nu = 3.763, 4.111$  and  $4.235$  for  $n_e = 3n_0, 5n_0$  and  $7n_0$ , respectively, when  $\alpha = 0$ . On the other hand, we find  $\nu = 2.829, 3.203$  and  $3.433$  for  $n_e = 3n_0, 5n_0$  and  $7n_0$ , respectively, when  $\alpha = \alpha_0$ . The exponent  $\nu$  is increasing with electron density.

In the high temperature limit around  $T = (18 - 40)$  K, we get  $\nu = 0.824, 0.998$  and  $1.019$  for densities  $n_e = 3n_0, 5n_0$  and  $7n_0$ , respectively. The  $\nu$  is also increasing with  $n_e$  slowly and the equipartition result  $\rho \sim T$  is re-

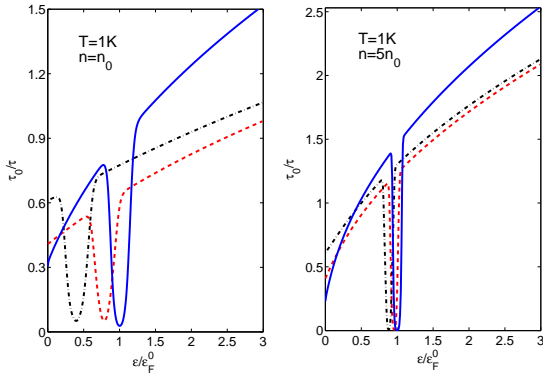


FIG. 1: (Color online) Plots of the IRT [in units of  $1/\tau_0 = 2m^*D^2\sqrt{2\pi n_0}/(\pi\hbar^2\rho_a v_s)$ ] versus energy for different values of  $\alpha$ . The solid, dashed and dot-dashed lines correspond to the  $\alpha = 0$ ,  $\alpha = 3\alpha_0$  and  $\alpha = 5\alpha_0$ , respectively. For better visualization, the solid lines in the left and the right panels have been reduced by a factor of 3 and 4, respectively.

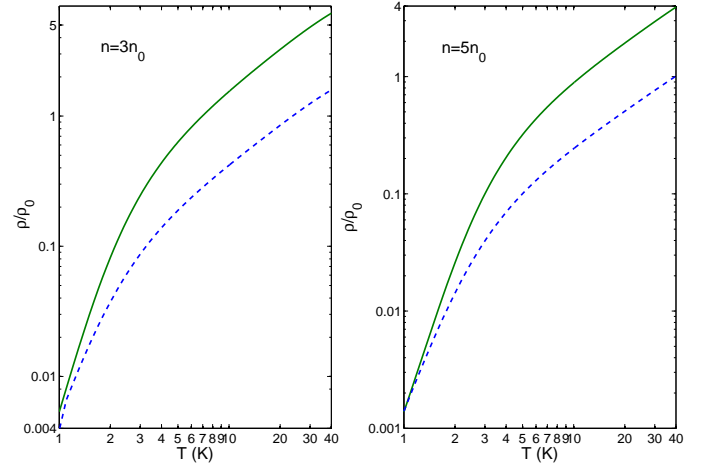


FIG. 3: (Color online) Plots of the resistivity with temperature at a fixed density for different values of  $\alpha$ . Here, solid and dashed lines correspond to the  $\alpha = 0$  and  $\alpha = \alpha_0$ , respectively.

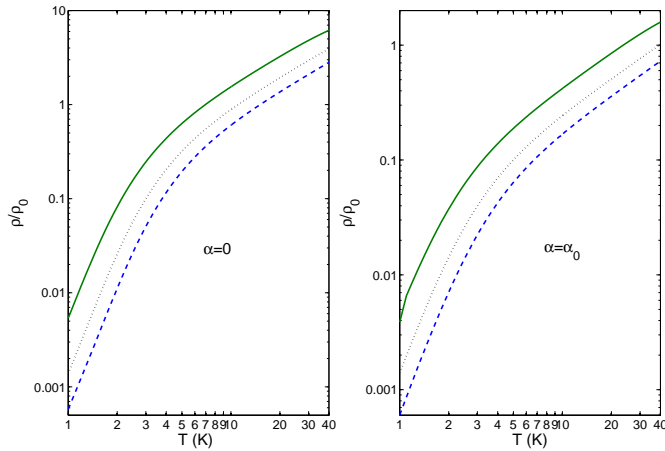


FIG. 2: (Color online) Plots of the resistivity [in units of  $\rho_0 = m^*/(n_0 e^2 \tau_0)$ ] of a perfect 2DEG versus  $T$  for  $\alpha = 0$  and  $\alpha = \alpha_0$  on a log-log scale. Here solid, dotted and dashed lines represent  $n_e = 3n_0$ ,  $n_e = 5n_0$  and  $n_e = 7n_0$ , respectively.

covered. The exponent  $\nu$  does not change due to  $\alpha$  in the high temperature limit.

In Fig. 3, we plot  $\rho$  versus  $T$  at a fixed density for different values of  $\alpha$ . In the each panel of Fig. 3, we consider  $\alpha = 0$  and  $\alpha = \alpha_0$  cases for densities  $n_e = 3n_0$  and  $n_e = 5n_0$ . Figure 3 clearly shows that the slope of the curve for  $\alpha = 0$  is greater than that for  $\alpha = \alpha_0$  case in the BG regime. When  $n_e = 3n_0$ , we estimate  $\nu = 3.763$  and  $\nu = 2.829$  for  $\alpha = 0$  and  $\alpha = \alpha_0$ , respectively. Similarly, when  $n_e = 5n_0$   $\nu = 4.111$  and  $\nu = 3.203$  for  $\alpha = 0$  and  $\alpha = \alpha_0$ , respectively, at very low temperature. The values of  $\nu$  differ significantly between  $\alpha = 0$  and finite

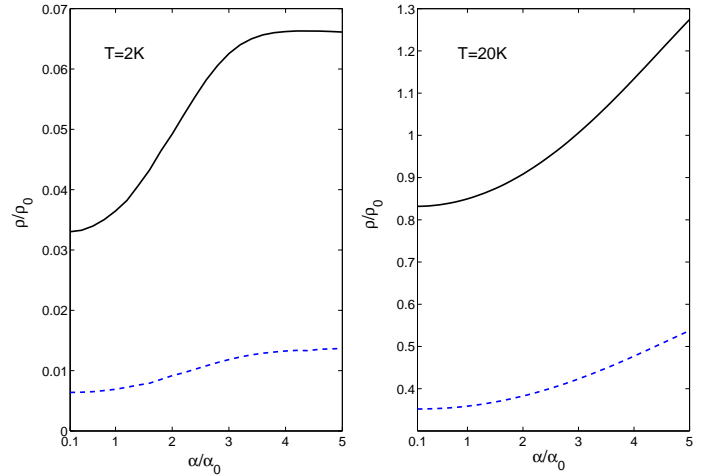


FIG. 4: (Color online) Plots of  $\rho$  of a perfect 2DEG versus  $\alpha$  for two fixed densities. Here solid and dashed lines correspond to  $n_e = 3n_0$  and  $n_e = 7n_0$ , respectively.

$\alpha$  at very low temperature.

In Fig. 4, we plot resistivity of a perfect 2DEG versus  $\alpha$  for two different densities. In both the regimes,  $\rho$  increases with  $\alpha$ . But the rate of increase of  $\rho$  is high for low electron density compared to that of the high density. In the BG regime, the resistivity is saturated at high  $\alpha$ .

### III. ELECTRON-PHONON SCATTERING IN A QUASI-2DEG

In this section we consider three dimensional bulk phonon with wave vector  $\mathbf{Q} = (\mathbf{q}, q_z)$  interacts with the two dimensional electron wave vector  $\mathbf{k} = (k_x, k_y)$ . The component of  $\mathbf{Q}$  in the  $xy$  plane obeys the conservation of momentum i.e  $\mathbf{k} - \mathbf{k}' = \mathbf{q}$  and the  $z$ -component must be integrated out. In semiconductor heterostructure the electrons move in the  $x$ - $y$  plane in presence of a triangular potential in the  $z$  direction. It is also assumed that the lowest energy level is occupied by the electrons. Generally the wave function can be written as  $\psi(\mathbf{r}) = \psi(x, y)\zeta_0(z)$ . Here the variational wave function  $\zeta_0(z)$  is given by,  $\zeta_0(z) = \sqrt{b^3/2z}e^{-bz/2}$ . The variational parameter<sup>38</sup>  $b$  is given by  $b = (48\pi m^* e^2 / \epsilon_0 \kappa_0 \hbar^2)^{1/3} (n_c + 11n_e/32)^{1/3}$ , where  $\kappa_0 = 12.9$  is the static dielectric constant of GaAs,  $\epsilon_0$  is the free space permittivity and  $n_c$  is the depletion charge density in the channel. In this section we will also discuss the piezoelectric scattering along with the deformation potential scattering. In this case the IRT can be written as

$$\begin{aligned} \frac{1}{\tau^\lambda(\epsilon)} &= \frac{1}{(2\pi)^3} \frac{2\pi}{\hbar} \sum_{\lambda'} \int dk' k' \int d\theta (1 - \cos\theta) \\ &\times \int dq_z |I(q_z)|^2 |C_{\mathbf{q}, q_z}^{\lambda, \lambda'}|^2 \left\{ N_Q \delta(\epsilon'_{\lambda'} - \epsilon_\lambda - \hbar\omega_Q) \right. \\ &\left. + (N_Q + 1) \delta(\epsilon'_{\lambda'} - \epsilon_\lambda + \hbar\omega_Q) \right\} \frac{1 - f(\epsilon'_{\lambda'})}{1 - f(\epsilon_\lambda)}, \quad (16) \end{aligned}$$

where the term  $|I(q_z)|^2$ , called the form factor, is responsible for getting transition rate from three dimensional bulk phonon state to two dimension. The exact form of this term for a triangular potential is given by  $|I(q_z)|^2 = |\int dz \zeta_0^2(z) e^{iq_z z}|^2 = b^6 / (b^2 + q_z^2)^3$ .

#### A. Deformation potential scattering

The matrix element in this case is given by

$$|C_{\mathbf{q}, q_z}^{\lambda, \lambda'}|^2 = \frac{D^2 \hbar Q}{2\rho_m v_s} \frac{1 + \lambda\lambda' \cos\theta}{2}, \quad (17)$$

where  $\rho_m$  is the mass density. At high temperature, we have  $N_Q \simeq N_Q + 1 \simeq k_B T / (\hbar v_s Q)$ . Inserting this matrix element into Eq. (16), we get

$$\begin{aligned} \frac{1}{\tau^\pm(\epsilon)} &\simeq \frac{2m^* D^2}{\pi^2 \hbar^3 \rho_m v_s^2} \left( 1 \mp \sqrt{\frac{\epsilon_\alpha}{\epsilon + \epsilon_\alpha}} \right) k_B T \\ &\times \int_0^1 dx x^2 \sqrt{1 - x^2} \int_0^\infty dq_z |I(q_z)|^2, \quad (18) \end{aligned}$$

with  $x = q/2k$ . Performing the integrations over  $x$  and  $q_z$ , we finally obtain the total IRT in the EP regime for

DP scattering as given by

$$\frac{1}{\tau(\epsilon)} = \frac{3}{32} \frac{m^* b D^2}{\rho_m \hbar^3 v_s^2} k_B T. \quad (19)$$

On the other hand, in the BG regime, we obtain the following expression for the energy averaged IRT (see appendix A1):

$$\left\langle \frac{1}{\tau^\pm} \right\rangle_{DP} \simeq \frac{D_0}{4} \left( 1 \mp \sqrt{\frac{\epsilon_\alpha}{\epsilon_F^0 - \epsilon_\alpha}} \right) \frac{D^2}{\rho_m v_s} \frac{5! \zeta(5)}{(v_s \hbar)^5} \frac{(k_B T)^5}{(k_F^\pm)^3}, \quad (20)$$

where  $\zeta(5) = 1.037$ .

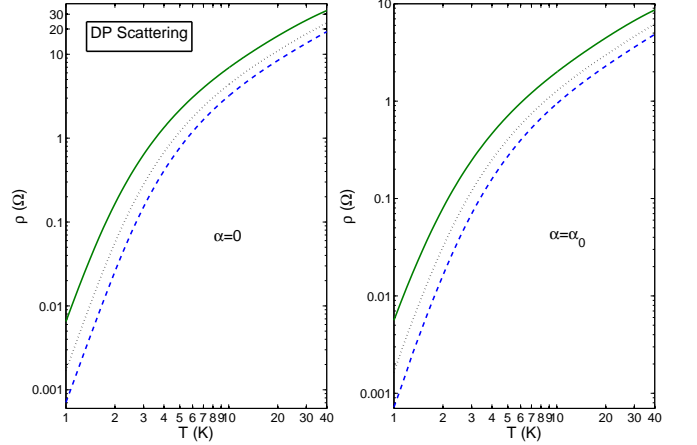


FIG. 5: (Color online) Plots of the resistivity of a quasi-2DEG due to DP scattering versus temperature for different values of the density. Here, solid, dotted and dashed lines represent  $n_e = 3n_0$ ,  $n_e = 5n_0$  and  $n_e = 7n_0$ , respectively.

#### B. Piezoelectric scattering

Piezoelectricity is nothing but generation of polarization due to the application of a strain to a crystal without inversion symmetry. Due to lattice vibration a potential can be generated in such crystals and electrons are scattered by this kind of potential. To calculate the IRT due to the PE scattering, we can use Eq. (16). Following Ref.<sup>25</sup>, the matrix elements of the Rashba system are obtained as

$$|C_{\mathbf{q}, q_z, l(t)}^{PE, \lambda, \lambda'}|^2 = \frac{(eh_{14})^2 \hbar}{2\rho_m v_{sl(t)}} \frac{1 + \lambda\lambda' \cos\theta}{2\sqrt{q^2 + q_z^2}} A_{l(t)}(\mathbf{q}, q_z), \quad (21)$$

where  $A_l(\mathbf{q}, q_z) = 9q_z^2 q^4 / 2(q_z^2 + q^2)^3$  and  $A_t(\mathbf{q}, q_z) = (8q_z^4 q^2 + q^6) / 4(q_z^2 + q^2)^3$ . In Eq. (21) the value PE tensor component  $h_{14}$  is  $1.2 \times 10^9$  V/m and  $v_{sl(t)}$  is the longitudinal (transverse) component of sound velocity. By inserting this matrix element into Eq. (16) and doing

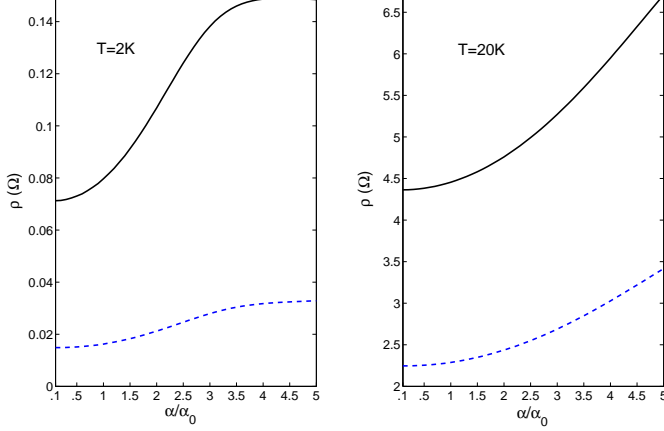


FIG. 6: (Color online) Plots of the resistivity of a quasi-2DEG due to DP scattering versus  $\alpha$  for various densities. Here, solid and dashed lines correspond to  $n_e = 3n_0$  and  $n_e = 7n_0$ , respectively.

some straightforward calculations in the high temperature regime we get,

$$\frac{1}{\tau_l^\pm(\epsilon)} \simeq \frac{9}{8\pi^2} \frac{m^*}{\hbar^3} \frac{(eh_{14})^2}{\rho_m v_{st}^2} \left(1 \mp \sqrt{\frac{\epsilon_\alpha}{\epsilon + \epsilon_\alpha}}\right) k_B T \times \int_0^\pi d\theta \sin^2 \theta F_l(q) \quad (22)$$

and

$$\frac{1}{\tau_t^\pm(\epsilon)} \simeq \frac{1}{16\pi^2} \frac{m^*}{\hbar^3} \frac{(eh_{14})^2}{\rho_m v_{st}^2} \left(1 \mp \sqrt{\frac{\epsilon_\alpha}{\epsilon + \epsilon_\alpha}}\right) k_B T \times \int_0^\pi d\theta \sin^2 \theta F_t(q). \quad (23)$$

Here  $F_l(q)$  and  $F_t(q)$  are respectively given by

$$F_l(q) = \int dq_z |I(q_z)|^2 \frac{q_z^2 q^4}{(q_z^2 + q^2)^4} = \frac{\pi}{16q} \frac{1 + 6\kappa + 12\kappa^2 + 2\kappa^3}{(1 + \kappa)^6} \quad (24)$$

and

$$F_t(q) = \int dq_z |I(q_z)|^2 \frac{8q_z^4 q^2 + q^6}{(q_z^2 + q^2)^4} = \frac{\pi}{16q} \times \frac{13 + 78\kappa + 72\kappa^2 + 82\kappa^3 + 36\kappa^4 + 6\kappa^5}{(1 + \kappa)^6}, \quad (25)$$

where  $\kappa = q/b$ . Now, we are assuming that the quasi-2DEG is very thin, i.e.  $\kappa \ll 1$ . So  $F_l(q)$  and  $F_t(q)$  can be approximated as  $F_l(q) \simeq \pi/16q$  and  $F_t(q) \simeq 13\pi/16q$ .

Substituting  $F_l(q)$ ,  $F_t(q)$  and  $q = 2k \sin(\theta/2)$  in Eqs. (22) and (23) and integrating over  $\theta$ , we obtain

$$\frac{1}{\tau_l^\pm(\epsilon)} \simeq \frac{3}{32} \frac{m^*}{\pi \hbar^3} \frac{(eh_{14})^2}{\rho_m v_{st}^2} \frac{1}{k^\pm} \left(1 \mp \sqrt{\frac{\epsilon_\alpha}{\epsilon + \epsilon_\alpha}}\right) k_B T \quad (26)$$

and

$$\frac{1}{\tau_t^\pm(\epsilon)} \simeq \frac{13}{192} \frac{m^*}{\pi \hbar^3} \frac{(eh_{14})^2}{\rho_m v_{st}^2} \frac{1}{k^\pm} \left(1 \mp \sqrt{\frac{\epsilon_\alpha}{\epsilon + \epsilon_\alpha}}\right) k_B T. \quad (27)$$

The total IRT for longitudinal and transverse cases are given as

$$\frac{1}{\tau_l(\epsilon)} \simeq \frac{3}{16} \frac{m^*}{\pi \hbar^3} \frac{(eh_{14})^2}{\rho_m v_{st}^2} \frac{k_B T}{k_F^0} \sqrt{\frac{\epsilon_F^0}{\epsilon + \epsilon_\alpha}} \quad (28)$$

and

$$\frac{1}{\tau_t(\epsilon)} \simeq \frac{13}{96} \frac{m^*}{\pi \hbar^3} \frac{(eh_{14})^2}{\rho_m v_{st}^2} \frac{k_B T}{k_F^0} \sqrt{\frac{\epsilon_F^0}{\epsilon + \epsilon_\alpha}}. \quad (29)$$

The total IRT in the PE scattering case can be written as  $1/\tau^{PE} = 1/\tau_l + 2/\tau_t$ . In the high temperature regime, the IRT is proportional to  $k_B T$  and inversely proportional to  $\sqrt{\epsilon + \epsilon_\alpha}$ .

In the low temperature regime we calculate IRT averaged over energy. The detail calculations are given in appendix A2. In this case, we have following expressions

$$\left\langle \frac{1}{\tau_l^\pm} \right\rangle_{PE} \simeq \frac{45}{512} \frac{m^*}{\pi \hbar} \frac{(eh_{14})^2}{\rho_m} \frac{3! \zeta(3)}{(\hbar v_{st})^4} \left(\frac{k_B T}{k_F^\pm}\right)^3 \times \left(1 \mp \sqrt{\frac{\epsilon_\alpha}{\epsilon_F^0 - \epsilon_\alpha}}\right) \quad (30)$$

and

$$\left\langle \frac{1}{\tau_t^\pm} \right\rangle_{PE} \simeq \frac{59}{1024} \frac{m^*}{\pi \hbar} \frac{(eh_{14})^2}{\rho_m} \frac{3! \zeta(3)}{(\hbar v_{st})^4} \left(\frac{k_B T}{k_F^\pm}\right)^3 \times \left(1 \mp \sqrt{\frac{\epsilon_\alpha}{\epsilon_F^0 - \epsilon_\alpha}}\right). \quad (31)$$

Here,  $\zeta(3) = 1.202$ . Equations (30) and (31) show that the energy averaged IRT due to PE scattering is proportional to  $T^3$  and hence the resistivity is also proportional to  $T^3$ .

### C. Numerical results

In this section we discuss resistivity due to both DP and PE scattering mechanisms. We solve Eq. (16) numerically using the matrix elements for DP and PE scattering given in Eqs. (17) and (21), respectively. For the numerical calculation we set  $v_{sl} = 5.31 \times 10^3 \text{ ms}^{-1}$ ,  $v_{st} = 3.04 \times 10^3 \text{ ms}^{-1}$ ,  $n_c = 5 \times 10^{14} \text{ m}^{-2}$ ,  $\rho_m = 5.12 \times 10^3 \text{ Kgm}^{-3}$  and  $D = 12 \text{ eV}$ . The other parameters are the same as given in Sec. II. The values of the numerical parameters considered in this section and also in Sec. II are appropriate for GaAs/AlGaAs heterostructure. These material parameters are different for different kind of heterostructures.

In Fig. 5, we show the temperature dependence of the resistivity of the quasi-2DEG due to the DP scattering for

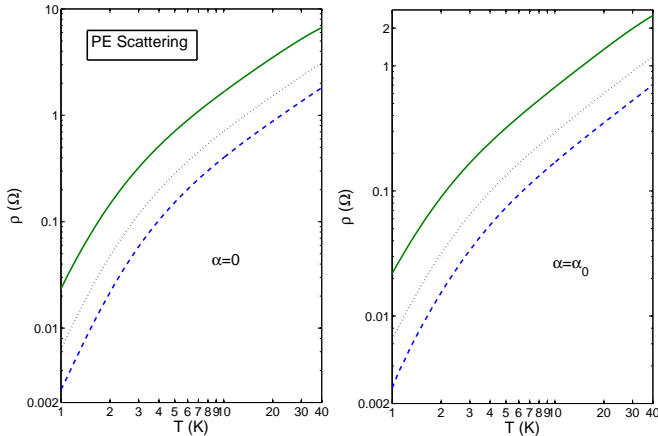


FIG. 7: (Color online) Plots of the resistivity due to PE scattering versus temperature for different values of the density. Here, solid, dotted and dashed lines represent  $n_e = 3n_0$ ,  $n_e = 5n_0$  and  $n_e = 7n_0$ , respectively.

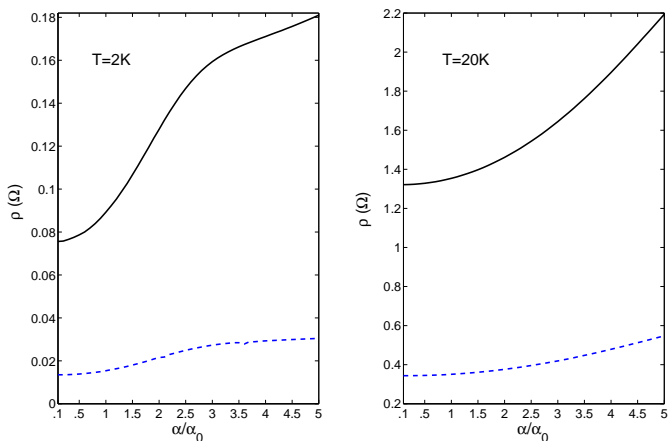


FIG. 8: (Color online) Plots of the resistivity of a quasi-2DEG due to piezoelectric scattering versus  $\alpha$  for various densities. Here, solid and dashed lines correspond to  $n_e = 3n_0$  and  $n_e = 7n_0$ , respectively.

fixed values of  $\alpha = 0$  and  $\alpha = \alpha_0$  with different densities. In the BG regime with  $\alpha = 0$ , the effective exponents of  $T$  are  $\nu = 4.459, 4.887$  and  $5.085$  for densities  $n_e = 3n_0, 5n_0$  and  $7n_0$ , respectively. Similarly, for  $\alpha = \alpha_0$ , we get the exponents as  $\nu = 3.6499, 4.058$  and  $4.359$  for densities  $n_e = 3n_0, 5n_0$  and  $7n_0$ , respectively. In this case,  $\nu$  is greater than the perfect 2DEG case discussed in the previous section. This increase in  $\nu$  is due to the finite thickness of quasi-2DEG in the  $z$  direction. In the EP regime, the  $\nu$  is closed to one as we increase  $n_e$ .

In Fig. 6, we plot the resistivity of a quasi-2DEG due to DP scattering as a function of  $\alpha$  at fixed temperature

and density. Figure 6 shows that the  $\rho$  increases rapidly with  $\alpha$  in both the regimes but it is faster for low electron density and gets saturated after certain value of  $\alpha$  in the BG regime.

In Fig. 7, we plot the temperature dependence of the resistivity of the quasi-2DEG due to the PE scattering for fixed values of  $\alpha = 0$  and  $\alpha = \alpha_0$  with different densities. When  $\alpha = 0$ , the exponents are  $\nu = 2.537, 2.830$  and  $3.002$  for densities  $n_e = 3n_0, 5n_0$  and  $7n_0$ , respectively, in the BG regime. Similarly, the effective exponents are  $\nu = 1.962, 2.208$  and  $2.398$  for densities  $n_e = 3n_0, 5n_0$  and  $7n_0$ , respectively, when  $\alpha = \alpha_0$ . It clearly shows that the exponent  $\nu$  is decreased due to the presence of the RSOI.

For PE scattering case we also calculate the resistivity of a quasi-2DEG as a function of  $\alpha$  by solving Eq. (16) and plot the results in Fig. 8. Figure 8 shows that  $\rho$  increases with  $\alpha$  in both the regimes. The other features are similar to the DP scattering mechanism.

Comparing Fig. 6 and Fig. 8, one could see that the resistivity due to DP and PE potential are in the same order in the BG regime but  $\rho$  due to DP is dominating over PE in the EP regime.

In past most studies regarding phonon-limited transport phenomena in heterostructures without spin-orbit interaction have been performed by focusing on mobility instead of resistivity. Our results for  $\alpha = 0$  case are consistent with those previous results.

#### IV. SUMMARY

In this work we have investigated the effect of the Rashba spin-orbit interaction on the momentum relaxation time due to the electron-phonon scattering in a 2DEG. We have considered both perfect 2DEG and quasi-2DEG. We have also considered both the deformation potential and piezoelectric scattering mechanisms responsible for the electron-phonon interaction separately. The temperature dependence of the resistivity has been calculated in both equipartition and Bloch-Gruneisen regimes. We have found through approximate calculations that the resistivity of a perfect 2DEG is proportional to  $T^4$  in the Bloch-Gruneisen regime for the deformation potential scattering. On the other hand,  $\rho \sim T^5$  for deformation potential scattering and  $\rho \sim T^3$  for piezoelectric scattering in a quasi-2DEG. We have also recovered the linear temperature dependence of the resistivity in the equipartition regime of all the cases. Our numerical analysis showed that the effective exponent ( $\nu$ ) of the temperature dependence of the resistivity *strongly* depends on the electron density  $n_e$  and spin-orbit coupling constant  $\alpha$ . For the deformation potential and piezoelectric scattering, the values of the effective exponent of  $T$  in the Bloch-Gruneisen regime for different values of  $n_e$  and  $\alpha$  are summarized in Table I.

There is a reduction in the exponent of temperature dependence of resistivity in Bloch-Gruneisen regime due

Density ( $n_e$ )	$\nu$ for 2DEG		$\nu$ for quasi-2DEG			
	DP		DP		PE	
	$\alpha = 0$	$\alpha = \alpha_0$	$\alpha = 0$	$\alpha = \alpha_0$	$\alpha = 0$	$\alpha = \alpha_0$
$3n_0$	3.763	2.829	4.459	3.649	2.537	1.962
$5n_0$	4.111	3.203	4.887	4.058	2.830	2.208
$7n_0$	4.235	3.433	5.085	4.359	3.002	2.398

TABLE I: The effective exponent of the temperature dependence of the resistivity in the Bloch-Gruneisen regime for various values of  $n_e$  and  $\alpha$ .

to Rashba spin-orbit interaction at fixed electron density. We believe that the reduction in the exponent can be verified experimentally in near future.

The variation of  $\rho$  with  $\alpha$  has also been discussed for all the cases. It is found that the  $\rho$  increases with  $\alpha$  in both the regimes. The rate of increase is faster in low electron density case.

## Appendix A

In this appendix, we derive energy-averaged IRT due to DP and PE scattering in a quasi-2DEG in the BG regime. At very low temperature, following the approximations used in section II(A) and using Eq. (16), we get

$$\left\langle \frac{1}{\tau^\pm} \right\rangle \simeq \frac{m^*}{\pi^2 \hbar^3} \left( 1 \mp \sqrt{\frac{\epsilon_\alpha}{\epsilon_F^0 - \epsilon_\alpha}} \right) \frac{1}{k_B T} \int_0^\pi d\theta (1 - \cos \theta) \times \int dq_z |I(q_z)|^2 |C_{\mathbf{q}, q_z}|^2 \hbar \omega_Q N_Q (N_Q + 1). \quad (\text{A1})$$

When  $T$  is very low, the phonon wave vector  $q$  is very very small compared to the Fermi wave vector i.e.  $q \ll 2k_F$ . For very thin quasi-2DEG,  $|I(q_z)|^2$  can be approximated as  $|I(q_z)|^2 \simeq 1$  since  $q_z \ll b$ . With all the approximations taken into account, Eq. (A1) can be approximated further as

$$\left\langle \frac{1}{\tau^\pm} \right\rangle \simeq \frac{m^*}{2\pi^2 \hbar^3} \frac{1}{k_F^{\pm 3}} \left( 1 \mp \sqrt{\frac{\epsilon_\alpha}{\epsilon_F^0 - \epsilon_\alpha}} \right) \frac{1}{k_B T} \times \int dq dq_z q^2 |C_{\mathbf{q}, q_z}|^2 \hbar \omega_Q N_Q (N_Q + 1). \quad (\text{A2})$$

### 1. Deformation Potential scattering

Inserting the matrix element given in Eq. (17) into Eq. (A2), we get

$$\left\langle \frac{1}{\tau^\pm} \right\rangle_{DP} \simeq \frac{m^* D^2}{4\pi^2 \hbar^3 \rho_m v_s^2 k_F^{\pm 3}} \left( 1 \mp \sqrt{\frac{\epsilon_\alpha}{\epsilon_F^0 - \epsilon_\alpha}} \right) \frac{1}{k_B T} \times \int dq dq_z q^2 (\hbar \omega_Q)^2 N_Q (N_Q + 1). \quad (\text{A3})$$

Since the phonon dispersion relation is  $\epsilon_p = \hbar v_s \sqrt{q^2 + q_z^2}$ , we can make the following transformation:

$dq dq_z \rightarrow \epsilon_p d\epsilon_p d\phi / (\hbar v_s)^2$  with  $q = \epsilon_p \cos \phi / (\hbar v_s)$  and  $q_z = \epsilon_p \sin \phi / (\hbar v_s)$ . With these transformations, Eq. (A2) reduces to

$$\left\langle \frac{1}{\tau^\pm} \right\rangle_{DP} \simeq \frac{m^* D^2}{4\pi^2 \hbar^3 \rho_m v_s^2 k_F^{\pm 3}} \left( 1 \mp \sqrt{\frac{\epsilon_\alpha}{\epsilon_F^0 - \epsilon_\alpha}} \right) \frac{1}{(\hbar v_s)^4} \times \frac{1}{k_B T} \int d\epsilon_p \epsilon_p^5 N_Q (N_Q + 1). \quad (\text{A4})$$

Using the result  $\int d\epsilon_p \epsilon_p^n N_Q (N_Q + 1) = n! \zeta(n) (k_B T)^{n+1}$  with  $\zeta(n)$  is the Riemann zeta function, we finally obtain

$$\left\langle \frac{1}{\tau^\pm} \right\rangle_{DP} \simeq \frac{D_0}{4} \left( 1 \mp \sqrt{\frac{\epsilon_\alpha}{\epsilon_F^0 - \epsilon_\alpha}} \right) \frac{D^2}{\rho_m v_s} \frac{5! \zeta(5)}{(v_s \hbar)^5} \frac{(k_B T)^5}{(k_F^\pm)^3}. \quad (\text{A5})$$

### 2. Piezoelectric scattering

Using the matrix elements for PE scattering given in Eq. (21) and Eq. (A2), we obtain the energy-averaged IRT for longitudinal and transverse cases, respectively,

$$\left\langle \frac{1}{\tau_l^\pm} \right\rangle_{PE} \simeq \frac{9}{8\pi^2} \frac{m^* (eh_{14})^2}{\rho_m \hbar (\hbar v_{sl})^4 k_F^{\pm 3}} \left( 1 \mp \sqrt{\frac{\epsilon_\alpha}{\epsilon_F^0 - \epsilon_\alpha}} \right) \frac{1}{k_B T} \times \int d\epsilon_p \epsilon_p^3 N_Q (N_Q + 1) \int \cos^6 \phi \sin^2 \phi d\phi$$

and

$$\left\langle \frac{1}{\tau_t^\pm} \right\rangle_{PE} \simeq \frac{1}{8\pi^2} \frac{m^* (eh_{14})^2}{\rho_m \hbar (\hbar v_{st})^4 k_F^{\pm 3}} \left( 1 \mp \sqrt{\frac{\epsilon_\alpha}{\epsilon_F^0 - \epsilon_\alpha}} \right) \frac{1}{k_B T} \times \int (\cos^8 \phi + 8 \cos^4 \phi \sin^4 \phi) d\phi \times \int d\epsilon_p \epsilon_p^3 N_Q (N_Q + 1). \quad (\text{A6})$$

After doing the integration over  $\epsilon_p$  and  $\phi$ , we finally obtain the following expressions

$$\left\langle \frac{1}{\tau_l^\pm} \right\rangle_{PE} \simeq \frac{45}{512} \frac{m^* (eh_{14})^2}{\pi \hbar \rho_m} \frac{3! \zeta(3)}{(\hbar v_{sl})^4} \left( \frac{k_B T}{k_F^\pm} \right)^3 \times \left( 1 \mp \sqrt{\frac{\epsilon_\alpha}{\epsilon_F^0 - \epsilon_\alpha}} \right) \quad (\text{A7})$$

and

$$\left\langle \frac{1}{\tau_t^\pm} \right\rangle_{PE} \simeq \frac{59}{1024} \frac{m^* (eh_{14})^2}{\pi \hbar \rho_m} \frac{3! \zeta(3)}{(\hbar v_{st})^4} \left( \frac{k_B T}{k_F^\pm} \right)^3 \times \left( 1 \mp \sqrt{\frac{\epsilon_\alpha}{\epsilon_F^0 - \epsilon_\alpha}} \right). \quad (\text{A8})$$



- 
- <sup>1</sup> R. Winkler, Spin-Orbit Coupling Effects in Two-Dimensional Electron and Hole Systems (Springer Verlag-2003).
  - <sup>2</sup> F. Fabian, A. Matos-Abiague, C. Ertler, P. Stano, and I. Zutic, *Acta Physica Slovaca* **57**, 565 (2007).
  - <sup>3</sup> S. Bandyopadhyay and M. Cahay, *Introduction to Spintronics* (CRC press-2008).
  - <sup>4</sup> S. Datta and B. Das, *Appl. Phys. Lett.* **56**, 665 (1990).
  - <sup>5</sup> I. Zutic, J. Fabian, and S. Das Sarma, *Rev. Mod. Phys.* **76**, 323 (2004).
  - <sup>6</sup> S. A. Wolf, D. D. Awschalom, R. A. Burhman, J. M. Daughton, S. von Molnar, M. L. Roukes, A. Y. Chtchelkanova, and D. M. Treger, *Science*, **294**, 1488 (2001).
  - <sup>7</sup> D. D. Awschalom and M. E. Flatte, *Nature physics* **3**, 153 (2007).
  - <sup>8</sup> E. I. Rashba, *Fiz. Tverd. Tela (Leningrad)* **2**, 1224 (1960) [*Sov. Phys. Solid State* **2**, 1109 (1960)]; Y. A. Bychkov and E. I. Rashba, *J. Phys. C* **17**, 580 (1984).
  - <sup>9</sup> J. Nitta, T. Akazaki, H. Takayanagi, and T. Enoki, *Phys. Rev. Lett.* **78**, 1335 (1997).
  - <sup>10</sup> T. Matsuyama, R. Kursten, C. Meibner, and U. Merkt *Phys. Rev. B* **61**, 15588 (2000).
  - <sup>11</sup> G. Dresselhaus, *Phys. Rev.* **100**, 580 (1955).
  - <sup>12</sup> E. Cappelluti, C. Grimaldi, and F. Marsiglio, *Phys. Rev. B* **76**, 085334 (2007).
  - <sup>13</sup> E. Cappelluti, C. Grimaldi, and F. Marsiglio, *Phys. Rev. Lett.* **98**, 167002 (2007).
  - <sup>14</sup> A. V. Chaplik and L. I. Magarill, *Phys. Rev. Lett.* **96**, 126402 (2006).
  - <sup>15</sup> C. Grimaldi, E. Cappelluti, and F. Marsiglio, *Phys. Rev. Lett.* **97**, 066601 (2006).
  - <sup>16</sup> L. Chen, Z. Ma, J. C. Cao, T.Y. Zhang, and C. Zhang, *Appl. Phys. Lett.* **91**, 102115 (2007).
  - <sup>17</sup> Z. Li, Z. S. Ma, A. R. Wright, and C. Zhang, *Appl. Phys. Lett.* **90**, 112103 (2007).
  - <sup>18</sup> P. M. Krstajic, M. Pagano, and P. Vasilopoulos, *Physica E* **43**, 893 (2011).
  - <sup>19</sup> D. L. Rode and S. Knight, *Phys. Rev. B* **3**, 2534 (1971).
  - <sup>20</sup> C. Jiang, D. C. Tsui, and G. Weimann, *Appl. Phys. Lett.* **53**, 1533 (1988).
  - <sup>21</sup> A. Gold, *Appl. Phys. Lett.* **54**, 2100 (1989).
  - <sup>22</sup> A. Gold and T. Dolgoplov, *J. Phys.: Condens. Matter* **14**, 7091 (2002).
  - <sup>23</sup> O. Chalaev and D. Loss, *Phys. Rev. B* **80**, 035305 (2009).
  - <sup>24</sup> H. L. Stormer, L. N. Pfeiffer, K. W. Baldwin, and K. W. West, *Phys. Rev. B* **41**, 1278 (1990).
  - <sup>25</sup> P. J. Price, *Ann. Physics (N.Y)* **133** 217 (1981).
  - <sup>26</sup> P. J. Price, *J. Vac. Sci. Technol.* **19**, 599 (1981).
  - <sup>27</sup> P. J. Price, *Surf. Sci.* **113**, 199 (1982).
  - <sup>28</sup> B. K. Ridley, *J. Phys. C: Solid State Phys.* **15**, 5898 (1982).
  - <sup>29</sup> P. J. Price, *Surf. Sci.* **143**, 145 (1984).
  - <sup>30</sup> P. J. Price, *Solid State Commun.* **51**, 607 (1984).
  - <sup>31</sup> T. Kawamura and S. Das Sarma, *Phys. Rev. B* **45**, 3612 (1992).
  - <sup>32</sup> K. Kaasbjerg, Antti-Pekka Jauho, and K. S. Thygesen, arXiv: 1206:2003v1.
  - <sup>33</sup> E. H. Hwang and S. Das Sarma, *Phys. Rev. B* **77**, 115449 (2008).
  - <sup>34</sup> E. V. Castro, H. Ochoa, M. I. Katsnelson, R. V. Gorbachev, D. C. Elias, K. S. Novoselov, A. K. Geim, and F. Guinea, *Phys. Rev. Lett.* **105**, 266601 (2010).
  - <sup>35</sup> K. Kaasbjerg, K. S. Thygesen, and K. W. Jacobsen, *Phys. Rev. B* **85**, 165440 (2012).
  - <sup>36</sup> D. K. Efetov and P. Kim, *Phys. Rev. Lett.* **105**, 256805 (2010).
  - <sup>37</sup> F. Gao, D. J. D. Beaven, J. Fulcher, C. H. Yang, Z. Zeng, W. Xu, and C. Zhang, *Physica E* **40**, 1454 (2008).
  - <sup>38</sup> T. Ando, Alan B. Fowler, and F. Stern, *Rev. Mod. Phys.* **54**, 437 (1982).